High Resolution Multispectral Camera System for ERTS A & B

B. P. MILLER,* GEORGE A. BECK,† AND JOSEPH M. BARLETTA‡
RCA Astro-Electronics Division, Princeton, N. J.

A very high resolution multispectral television camera system has been developed for NASA for use on the Earth Resources Technology Satellite (ERTS) program. There are three cameras in the system, each viewing the same area but operating in the blue-green, red, and near-infrared spectral bands. In the laboratory the cameras' limiting resolution is 4500 TV lines over the 25 × 25-mm image format of the Return Beam Vidicon (RBV). Analysis of typical ERTS scenes shows that actual contrast ratios will be much lower than those of laboratory test targets. A model was developed to predict the resolving power performance of the RBV camera under realistic conditions. To verify the model, tests were conducted using the RBV camera, a laser-beam image reproducer and a series of AF tribar test patterns of known values of contrast. As a more graphic demonstration, simulated multispectral images were generated using color-IR photographs from Apollo 9. The measured signal-to-noise, resolution, and spectral characteristics of the ERTS Flight A and Flight B three-camera systems are presented in conclusion.

Introduction

THE Two-Inch (50.8 mm) Return-Beam Vidicon (RBV) Multispectral Three-Camera Subsystem is based on a very high resolution television camera developed for NASA§ for use on the Earth Resources Technology Satellite (ERTS). This paper includes a description of camera operation and camera characteristics, typical ERTS scenes expected, a theoretical analysis, and a multispectral simulation of typical ERTS scenes. Measured spectral and resolving power performance data for the ERTS A and B flight three-camera subsystems is also included. All of these items form a concise picture of the Three-Camera Subsystem and what can be expected of it during the ERTS mission.

RBV Camera Description

The three cameras of the subsystem are identical electronically, but each operates in a different spectral band. The spectral regions include the blue-green (0.475–0.575 μm), the red (0.58–68 μm), and the near IR (0.69–0.83 μm).

The heart of the camera is the return-beam vidicon. This tube employs an ASOS photoconductive surface and a unique electrooptical configuration to achieve high resolution and signal-to-noise (SNR) performance. The high resolution is achieved by using a fourth node, nonuniform focus field, and high SNR at the contemplated exposure levels is obtained by utilizing the return beam and an electron multiplier (similar to the image orthicon). To prepare the RBV for picture-taking, an erase cycle is initiated. This involves flashing four miniature lamps located on the periphery of the faceplate for approximately 0.5 sec to erase any residual image left on the photoconductor. Next the target is prepared by scanning the photoconductor with the electron beam so as to bring the photoconductor down to cathode potential. The exposure portion of the sequence may take from 4–16 msec, depending on the scene radiance. A focal-plane shutter is used to expose the photoconductor.

The final sequence is the read. Here the electron beam is used to read out the scene imaged on the photoconductor. The readout sequence takes 3.5 sec for each frame (one camera). With the Three-Camera Subsystem, the cameras are exposed simultaneously and read out sequentially. A configuration diagram of the RBV is shown in Fig. 1. A summary of the Three-Camera Subsystem characteristics is given in Table 1 (Ref. 1).

Scene Characteristics

The over-all mission of the ERTS program is to observe the surface of the Earth in several regions. Features of interest include plant life (crops or forests), soil, rocks and geological formations, water, shorelines, etc. Figure 2 is indicative of the types of spectral variation that can be expected for various substances as compiled from a number of sources such as

Table 1 Three-camera subsystem performance characteristics

TV lines/format	4500 (90 line pairs/mm)
Deflection & focus	Electromagnetic
Image size	1 × 1-in. (25.4 × 25.4-mm)
Diagonal field of view	15.9°
Lens *f*/number	2.8
Focal length	126 mm
Dynamic range	30 to 1
Highlight exposure	
Channel 1	0.78 μjoule/cm^2
Channel 2	0.78 μjoule/cm^2
Channel 3	1.2 μjoule/cm^2
Spectral characteristics	
Channel 1	0.475–0.575 μm
Channel 2	0.580–0.680 μm
Channel 3	0.690–0.830 μm
Video bandwidth	3.2 MHz
Exposure time	4 to 16 msec (selectable)
Three-camera cycle rate	25 sec
Peak signal/rms noise	
Channel 1	33 db
Channel 2	33 db
Channel 3	25 db
Average power (three-camera system)	172 w
Weight (three-camera system and baseplate)	195 lb (88.5 kg)

Received November 20, 1972; revision received May 23, 1973.
Index category: Data Sensing and Presentation or Transmission of Systems.

* Project Manager. Associate Fellow AIAA.

† Manager, Systems Engineering.

‡ Systems Engineer.

§ The work described in this paper was performed for the NASA Goddard Space Flight Center under Contracts NAS5-11621 and NAS5-21904. The support of the NASA technical officer, O. Weinstein, is gratefully acknowledged.

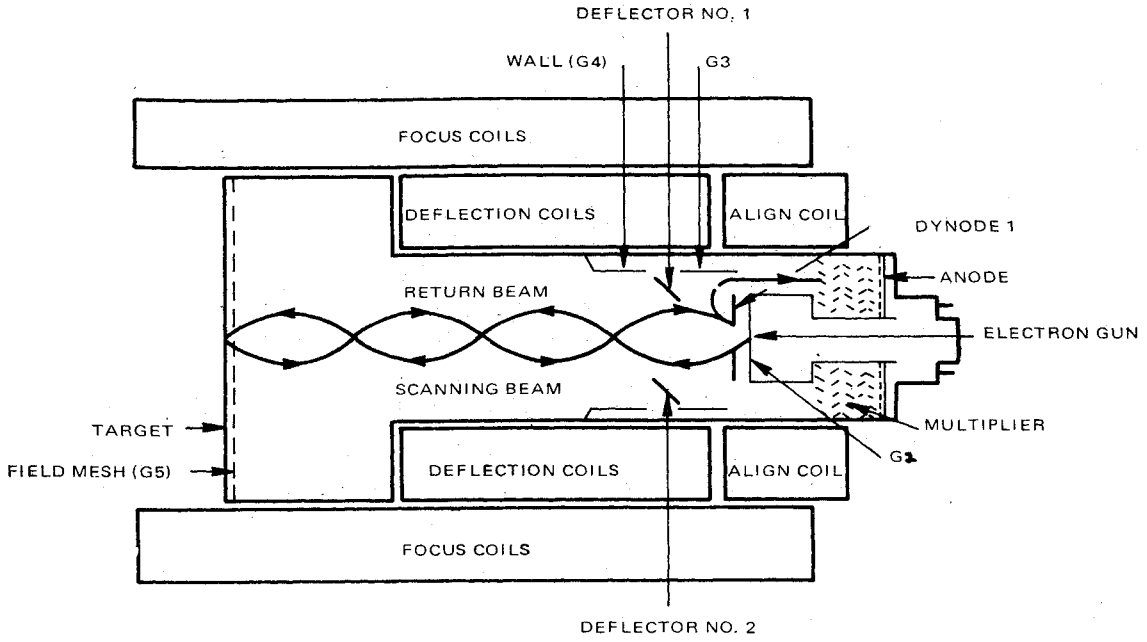

Fig. 1 Return beam vidicon (RBV) configuration diagram.

Ref. 2. Although certain substances have rather high reflectances, the majority of substances of interest, including most plant life, lie toward the low end of the reflectance scale. Full-scale settings indicated in Fig. 2 are values which permit optimizing performance for low reflectances. In operation there are options to select higher values of full-scale reflectance by commanding shorter exposure times for the cameras.

The radiance associated with a given substance as perceived by the cameras in space depends not only on the reflectance, but also on the incident energy and on effects of the atmosphere between scene and camera. The incident solar irradiance depends on the angle between the zenith at the scene and the irradiance itself. The scene irradiance is maximum when the sun is directly overhead (zero solar zenith angle), and falls off approximately as the cosine of the zenith angle. A zenith angle of 60° will be used for analysis: this is the worst lighting condition encountered over the 48 contiguous states in the U.S. during more than half of the year. To show what typical substances would look like as viewed from outside the atmosphere, the spectral reflectance data of Fig. 2 are combined with the characteristics of the atmosphere for a 60° solar zenith angle. Figure 3 shows the spectral radiances which result for these particular substances. Similar results are reported in Ref. 3. The radiance includes both reflected and scattered energy as seen by a camera in space looking vertically downward at the scene. The full-scale camera settings indicated in Fig. 3 correspond approximately to the reflectance values of Fig. 2.

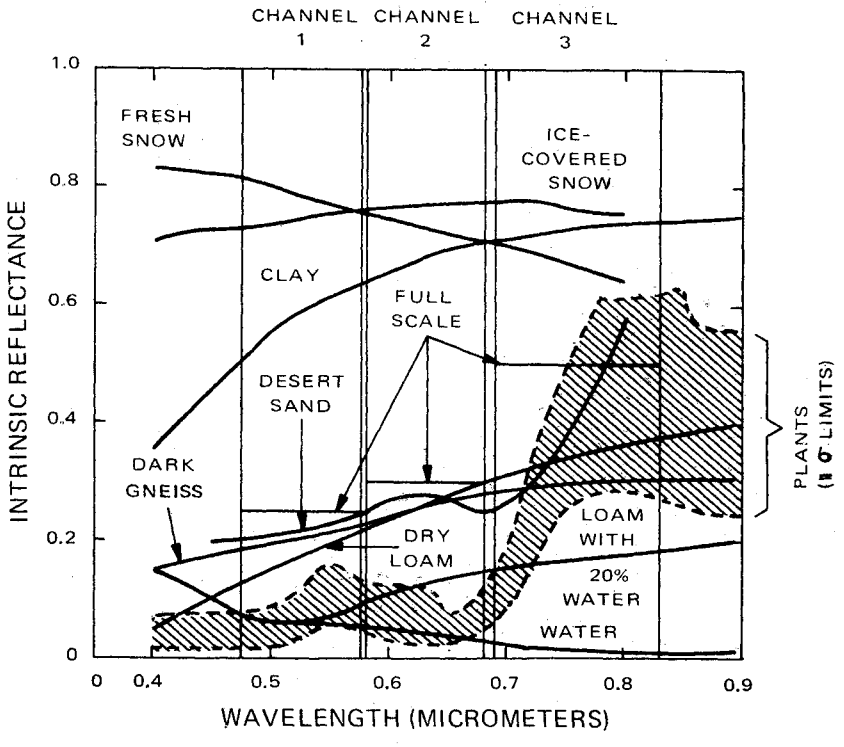

Fig. 2 Spectral reflectance of various substances.

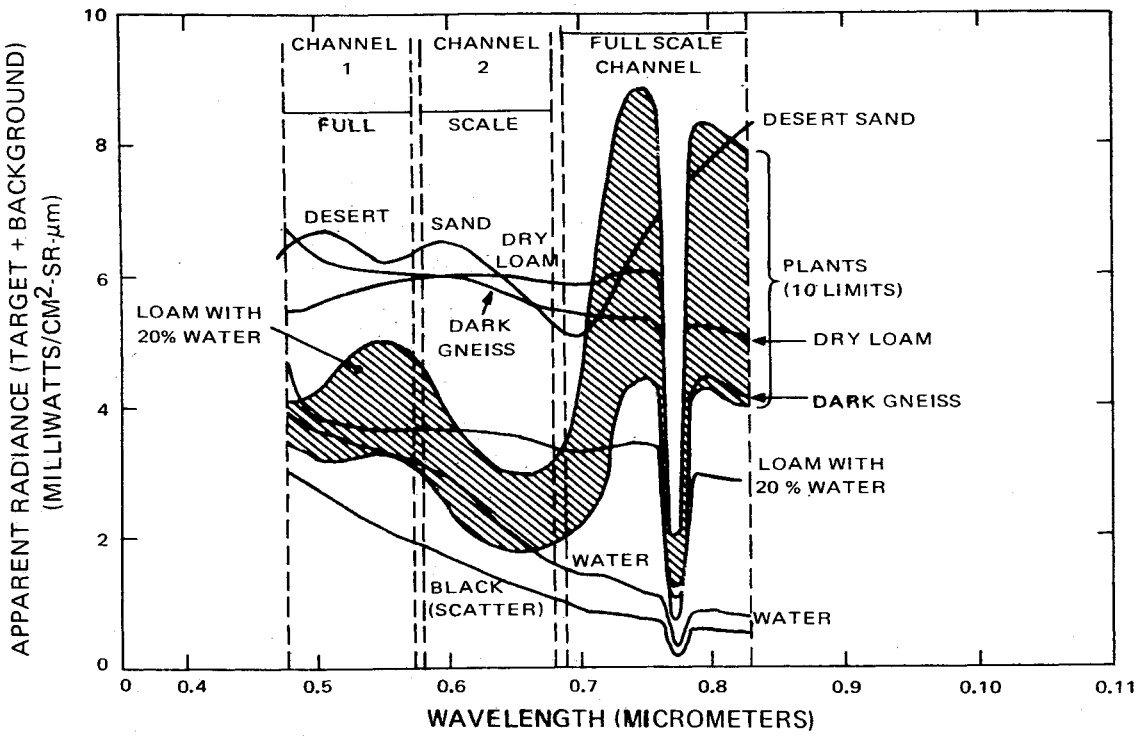

Fig. 3 Spectral radiances of typical substances looking vertically downward from space at 60° solar zenith angle.

The term "target" is used to denote a specific item of interest within the scene viewed by the camera. Within a scene, many targets of various sizes and shapes may be present, all characterized by a reflectance value differing from their immediate surrounding. The type of target used for analysis is the Air Force tribar pattern illustrated in Fig. 4. The size parameter is the spatial frequency f which is defined as the reciprocal of the combined width of one vertical bar and its adjacent space. The length of the bar l is 5 times its width w. The total scene has a range of radiance from N_{max} to N_{min}. Individual targets of interest may be supposed to consist of bars of radiance N_b in a surround of radiance N_a. The choice of $N_a > N_b$ for the illustration is arbitrary, N_a and N_b may take on any value in the range N_{min} to N_{max}. For analysis it is convenient to form the function mean radiance N and modulation M_0 which are defined as follows:

$$N = (N_a + N_b)/2$$
$$M_0 = |N_a - N_b|/(N_a + N_b)$$

For presentation of results the more familiar contrast ratio C will be used

$$C = N_a/N_b, \quad N_a > N_b$$
$$= N_b/N_a, \quad N_b > N_a$$

The contrast of some typical Earth Resources targets are listed in Table 2. Other more and less severe examples could be selected. The choices selected, however, are realistic and provide a good basis for evaluation of particular combinations of contrast and mean irradiance in the ERTS context. Reduced contrasts due to atmospheric effects are apparent from the entries, and higher contrasts are evident in channels 2 and 3. Values for a given target example, moreover, may vary widely from channel to channel. The "average plant vs wet loam" target, for example, would be undetectable in channel 1 but has sufficient contrast in channel 2 and 3 to allow reasonable probability of detection.

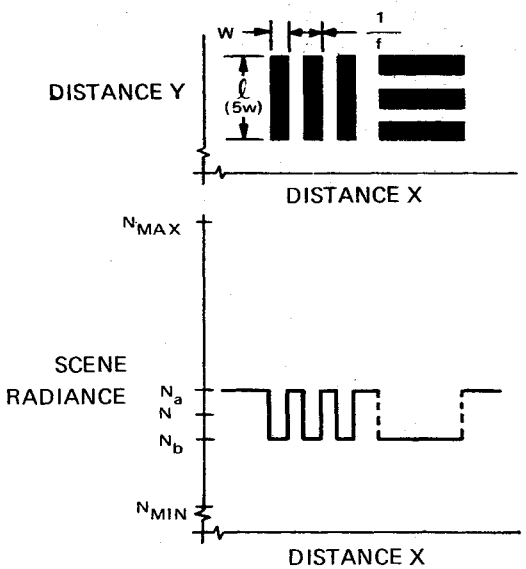

Fig. 4 Definition of target parameters.

Camera Characteristics

As is the case with any imaging system, the camera will degrade the contrast of small targets and will introduce noise. The contrast degradation can be ascertained by measuring the modulation transfer function of the camera. Figure 5 shows the square wave response of a typical RBV tube, from which the sine wave reponse of modulation transfer function (MTF) can be derived analytically.[9] The limiting resolution for a high-contrast target is seen to be about 90 cycles; i.e., 4500 TV lines over the 1-in. (25.4-mm) format.

A second parameter of the vidicon is its light-transfer characteristic (LTC), which relates voltage output scene radiance for mean levels or levels in large areas (near-zero spatial frequencies). The LTC is measured in a specific

Table 2 Scene characteristics

Channel	1	2	3
Wavelength interval (μm)	0.475–0.575	0.58–0.68	0.69–0.83
Total scene range:			
Desert sand reflectance	22%	27%	43%
Camera full-scale setting	25%	30%	50%
Contrast: full-scale	2:1 to	3:1 to	5:1 to
(with haze)	45:1	9:1	50:1
Typical targets			
Desert sand vs shadow:			
Ground contrast	∞	∞	∞
Space contrast	2.3:1	3.2:1	6.0:1
$+\sigma$ plant vs avg plant:			
Ground contrast	1.47:1	1.57:1	1.4:1
Space contrast	1.2:1	1.2:1	1.4:1
Avg plant vs $-\sigma$ plant:			
Ground contrast	1.90:1	2.29:1	1.57:1
Space contrast	1.2:1	1.4:1	1.5:1
Avg plant vs wet loam:			
Ground contrast	1.16:1	1.79:1	1.68:1
Space contrast	1.0:1	1.3:1	1.4:1
Avg plant vs dry loam:			
Ground contrast	2.18:1	3.72:1	1.05:1
Space contrast	1.5:1	2.2:1	1.3:1
Avg plant vs water:			
Ground contrast	1.32:1	1.79:1	19.9:1
Space contrast	1.1:1	2.2:1	3.4:1
Avg plant vs shadow:			
Ground contrast	∞	∞	∞
Space contrast	1.1:1	1.5:1	5.0:1

spectral band; incoming tubes are tested in all three channels. Figure 6 shows LTC curves for a typical tube. They are reasonably constant with a gamma of about 0.9. The noise contributed by the camera is measured with the beam current set to the minimum required to keep the LTC constant up to the specified full-scale radiance. Typical values of SNR for full-scale radiance are 33 db for channels 1 and 2 and 25 db for channel 3. The noise is assumed to be "white." with a frequency spectrum substantially constant over the band of interest.

Resolving Power Analysis

The data presented in the section on Camera Characteristics were concerned with high-contrast targets. The special test patterns also were designed to make the measurements convenient. The typical scene characteristics presented in Scene Characteristics section indicated that contrasts were low for targets of interest. The data do not permit a direct evaluation of camera performance for low-contrast targets; therefore, a method is needed to relate the laboratory results to what can be expected with real scenes. Target characteristics and several camera parameters all will be involved. The problem is to identify how various parameters involved affect performance, and to define what criterion can be used to determine resolving power.

A number of authors have addressed this problem for both television and photographic systems; Refs. 4 and 5 are typical. Generally the approach is to generate a model of the imaging system which computes the SNR for a low-contrast target as a function of the measured camera parameters. This SNR is then compared to an empirical threshold value to determine whether the target can be resolved.

The interaction of the various parameters in such a model is shown graphically in Fig. 7. The limiting spatial frequency is the unknown parameter. Target contrast establishes the value of modulation for low-frequency targets. Modulation is reduced, as a function of target frequency, in accordance with the camera MTF. The modulation required to resolve a target of a given size has been found[4–7] to be proportional to target spatial frequency; i.e., inversely proportional to target size. This implies that a given amount of noise is more effective in masking a small target than a large one. The effect is expressed analytically as a threshold value of signal to noise required to resolve a target; this threshold must then be adjusted for target size. The result is plotted on Fig. 7 as the curve marked "threshold modulation required." The vertical location of this curve is determined by 1) the mean exposure of the scene, 2) the camera gamma and SNR, and 3) the numerical value of the threshold criterion. The intersection of these two curves represents a balance between modulation available and modulation required, and therefore,

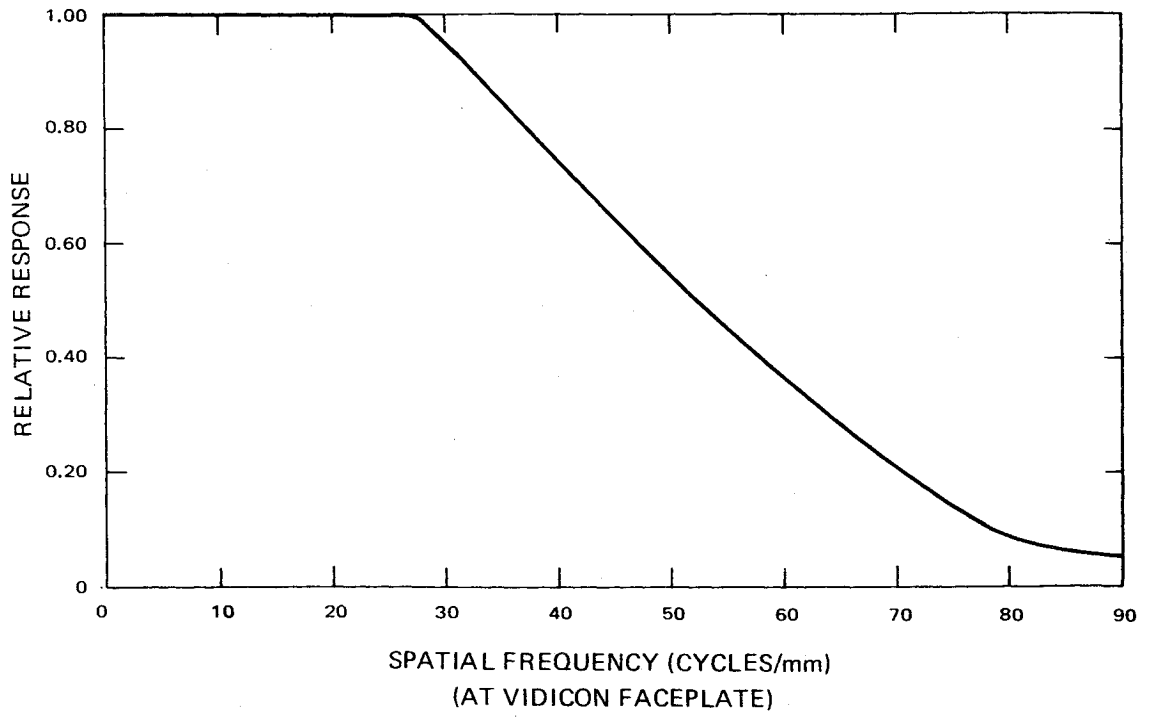

Fig. 5. Square wave response measured for vidicon and test lens.

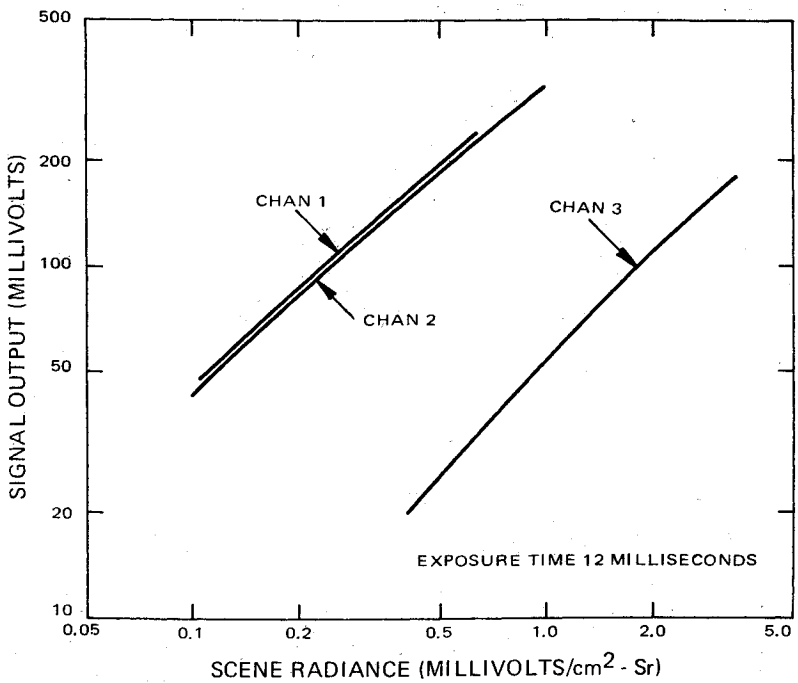

Fig. 6 Spectral light-transfer characteristics for typical return-beam vidicon.

indicates the resolving power (target spatial frequency which can just be resolved).

Variations in the parameters affect resolving power as follows.

1) Increased scene contrast raises the entire modulation-available curve, moving the intersection of the curves to the right. Resolving power improves for higher-contrast targets.

2) Improved camera MTF raises a portion of the modulation available curve, again increasing resolving power.

3) Increased mean exposure moves the threshold curve downward, with a given modulation representing a larger difference in level near full scale than near black. Resolving power, therefore, improves for targets near the full-scale portion of the scene.

4) Increased gamma (slope of the light transfer curve of Fig, 6) moves the threshold curve down, also improving resolving power. The gamma multiplies the actual modulation in the camera output.

5) Increased camera signal-to-noise ratio means less effect from noise and moves the threshold curve down, thus improving resolving power.

6) A higher threshold constant moves the threshold curve up and degrades resolving power.

The particular treatment that was used follows that of Schade.[8] It can be shown that the resolving power is the spatial frequency f, which satisfies the following expression:

$$\text{THRESH}/5^{1/2} = \text{SNR}\ (N/N_{\max})\gamma \times (2\gamma m_0)\ \bar{r}\ (f)\ (f_0/f)$$

where THRESH is the threshold SNR value, taken as 4.0[7]; SNR is the measured camera SNR referred to the full-scale signal radiance m max; N is the mean radiance of the target of interest; γ is the slope (log-log) of the measured light transfer characteristic of the camera; m_0 is the modulation of the target of interset; $\bar{r}$ is the average value of the square wave response of the camera[9]; f is the resolvable spatial frequency; and f_0 is the two-dimensional spatial bandwidth of the camera.

Resolving Power for the ERTS Mission

The preceding equation can be solved to find the resolvable frequency as a function of the scene parameters, contrast and mean radiance. The camera performance measurements are

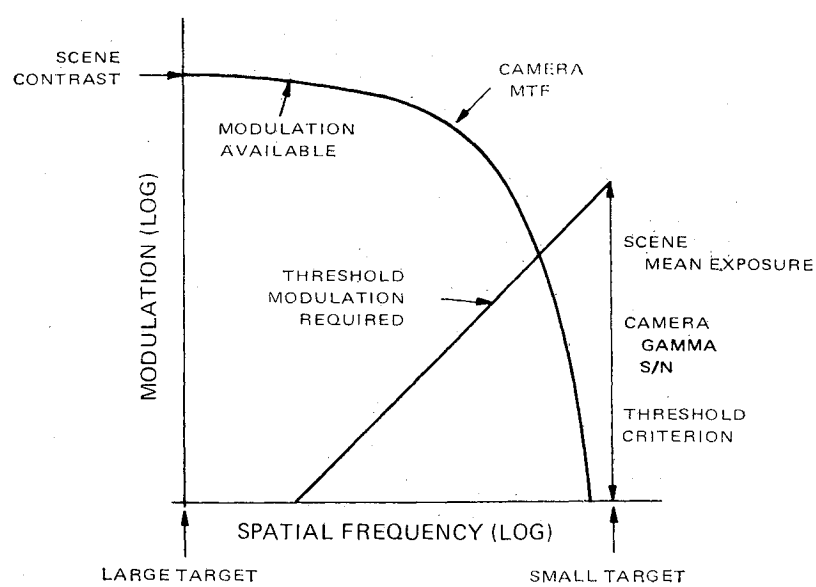

Fig. 7 Analytical model for resolving power analysis.

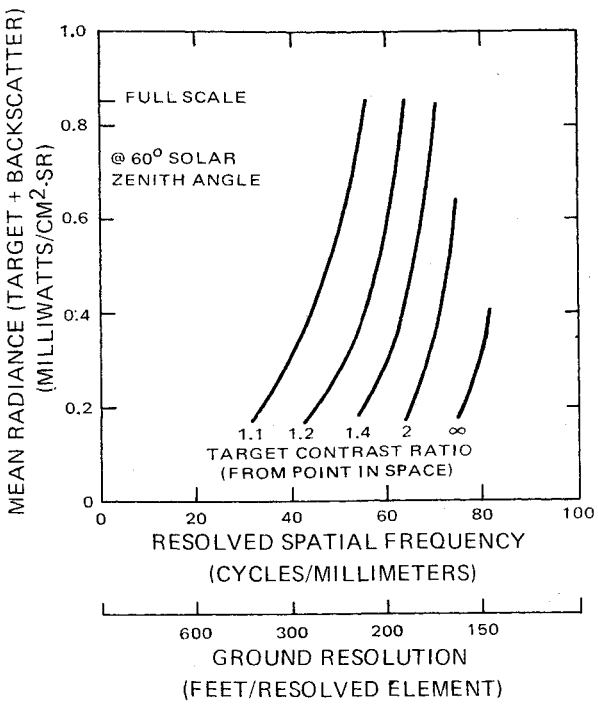

Fig. 8 RBV camera predicted revolving power, channels 1 and 2.

sufficient for this purpose, except for the effect of image motion during the exposure time. This motion is linear in a direction perpendicular to the scan lines and results in lower MTF in that direction. The approach taken was to make two sets of calculations, one using the measured MTF data and the second using the product of the measured MTF and a sin x/x function to account for the linear image motion. The results of these two calculations were averaged to obtain the estimated resolving power on-orbit.

The predicted performance of channels 1 and 2 is the same (Fig. 8), while channel 3 performance is somewhat lower due to the lower SNR (Fig. 9).

The resolvable target dimension ranged from approximately 150 ft (45 m) for high-contrast scenes to 500 ft (152 m) for low-contrast targets. The results in terms of typical ERTS mission targets are summarized in Table 3. These figures show the effects target contrast will have on the resolution obtained in each of the three spectral channels.

Low-Contrast Tests

In order to verify that the resolving power prediction technique is accurate, several tests were run in which the RBV camera was used to image low-contrast Air Force test targets.

Table 3 Typical target resolving power

Target	Avg ground resolution (ft/TV line)		
	Chan 1	Chan 2	Chan 3
High contrast (lab)	150	150	165
High contrast (scene, sand-shadow)	165	160	190
Typical plant-plant (1σ)	225	215	250
Avg plant—wet loam	∞	210	275
Avg plant—dry loam	180	165	275
Avg plant—water	275	275	205
Avg plant—shadow	200	210	200

In these tests, several RBV tubes were utilized with a Feasibility Model (preprototype) Camera. The camera video was sent to a Laser Beam Image Reproducer (LBIR)[10] which provided hard-copy photographs on 9-in (23-cm) film. The tubes used in these tests did not acheive the expected MTF and SNR performance. However, it was felt that, if the prediction theory was valid, it could still be demonstrated even with tubes of lower performance. With the MTF and SNR contribution of the LBIR entered into the analysis along with the RBV and target parameters, RBV camera performance was predicted as shown by the dashed lines in Fig. 10. This was compared to the actual observed limiting resolution on the film which was plotted on Fig. 10 in solid lines. The two sets of curves show good correlation well within the deviations that might be expected due to the inaccuracies in measuring all the various parameters (SNR, MTF, limiting resolution, etc.).

To prove the technique with an RBV having performance capabilities similar to the flight tubes, an additional low-contrast test was run with RBV 197. In Fig. 11 its SNR vs spatial frequency characteristics are compared to the target tubes. It can be seen from the curves that tube 197 has better performance at the higher spatial frequencies but that performance at the lower values is not as good. This resulted in resolving power capabilities as shown in Fig. 12. Here the solid lines represent the specified RBV performance as predicted in the previous section, but with the LBIR effects included. The dots are limiting resolutions actually seen on the RBV 197/LBIR film output. These sample points indicate that the design performance of the RBV was achieved with the higher contrast charts. It fell somewhat short of the design performance for the low contrast (1.22/1) chart because the tube 197 showed poorer capability at the lower spatial frequencies (Fig. 11). These are the frequencies which influence the performance of low-contrast scenes. The reduced performance of RBV 197 at lower spatial frequencies was later attributed to a slightly improper tube setup.

It can be concluded from all the low-contrast tests that the prediction theory appears accurate and that expected resolving power performance has been achieved.

Multispectral Photos

In addition to the low-contrast tests, a further measure of the performance of the Three-Camera Subsystem was obtained by imaging IR color scenes with a scale factor, spectral content and radiance similar to typical ERTS scenes.[11] Color balancing and registering these photos would give some indication of the difficulty that might be experienced in the operational system. The scenes used were taken on the Apollo 9 flight with 70 mm Kodak S0-180 IR color film (with Wrattan 15 filter). The IR film has a spectral sensitivity (see Fig. 13) similar to that of the Three-Camera Subsystem. The color negative transparencies of seven different scenes were utilized in the simulation. These scenes covered an area of approximately 75×75 naut miles ($138.9 \times 138.9 = 19{,}293$ km^2) and have an equivalent resolution capability across the active format of about 4000 TV lines.

The multispectral photos generated showed what typical scenes would look like when imaged with an ERTS RBV camera. Accurate sizing and proper scene registration were readily accomplished.

Camera Characteristics for ERTS Flight A and Flight B

Two flight qualified sets of multispectral Three-Camera Systems have been fabricated and their parameters measured. These camera systems are designated as Camera Group T and Camera Group F. Group T consists of TEM-1, which has channel 2 sensitivity, TEM 2 (channel 1), and TEM-3 (channel 3). Camera Group F includes F-1 (channel 2), F-2 (channel 3), and F-3 (channel 1). The only difference in the T and F

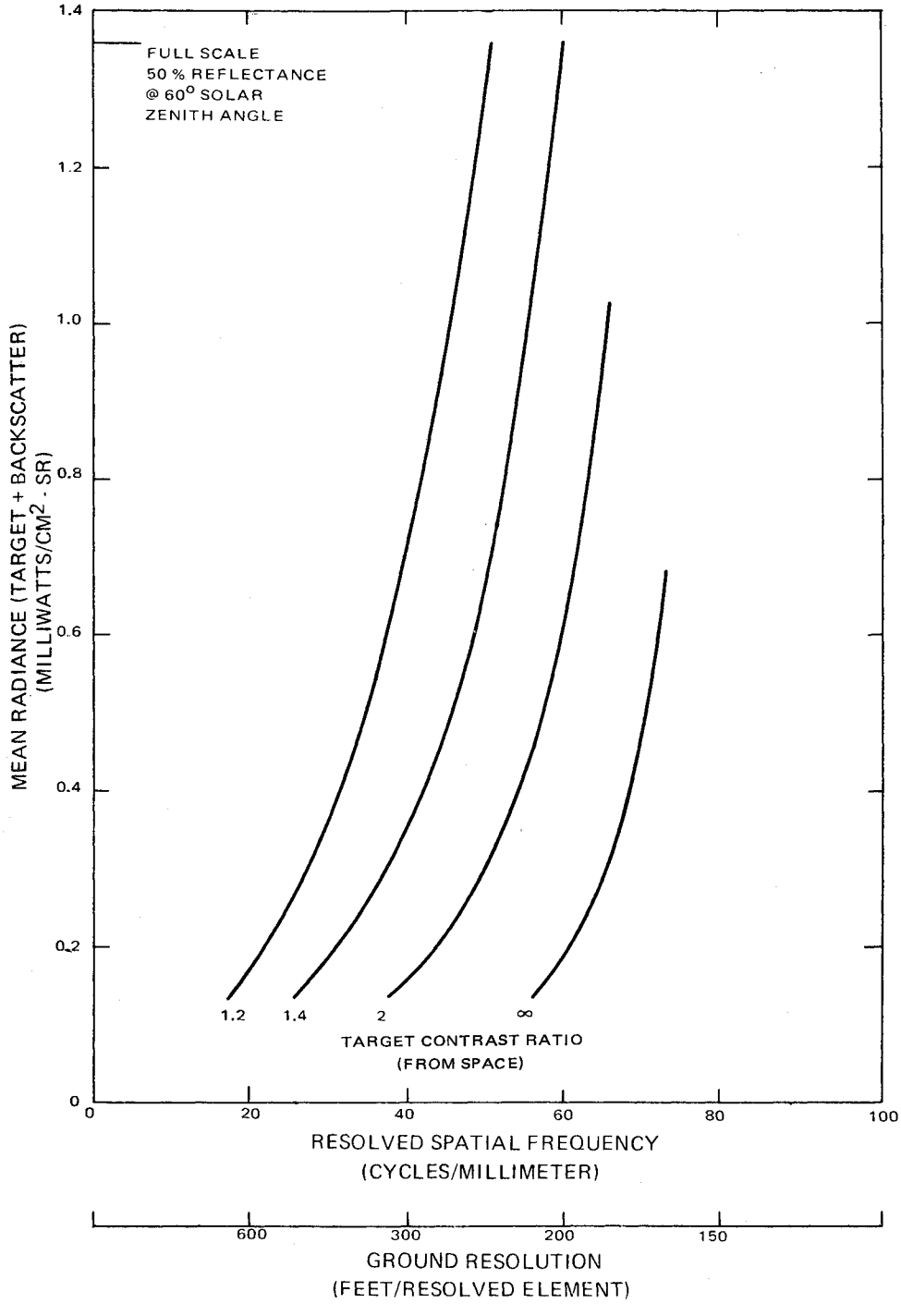

Fig. 9 RBV camera predicted revolving power, channel 3.

camera groups is in the details of the design of the RBV tubes used. Improvements principally in the areas of cathode and mesh construction were incorporated in the tubes used in the F group. The Group F cameras were flown in ERTS A. Although the vidicons in the Group T cameras will be replaced with tubes incorporating improved cathode and mesh construction prior to the Flight of ERTS B, the spectral and spatial characteristics of both groups of cameras are discussed to illustrate the relative uniformity of the performance achieved with the two sets of flight cameras.

The spectral characteristics of these two groups of cameras are given in Fig. 14. The small differences between the cameras are within the normal filter and photoconductor tolerances.

The relative imaging performance of the cameras may be discerned by looking at the signal-to-noise vs spatial frequency plots of Figs. 15 and 16. These plots were made by multiplying the SNR at low frequency by the square wave response of the camera. Since all the cameras have a gamma of approximately 0.9, cameras with a higher signal-to-noise at a particular spatial frequency will be better able to resolve those frequencies. The resolving power capability of TEM-1 (Fig. 15) therefore exceeds that of TEM-2 and TEM-3. It is also seen in the figures that in all cases the NASA limiting resolution spec of 90 LP/mm and the SNR spec of 33 db (channel 1 and 2) and 25 db (channel)3 are met.

The capability also exists for using aperture correction (frequency peaking) in the cameras. Aperture correction causes the cameras to have increased response at the higher spatial frequencies but results in a 3 to 4 db lower signal-to-noise ratio at zero spatial frequency. The SNR vs spatial frequency plots for the cameras with aperture correction show slightly larger SNR values at the higher spatial frequencies and smaller values at the low spatial frequencies. The total

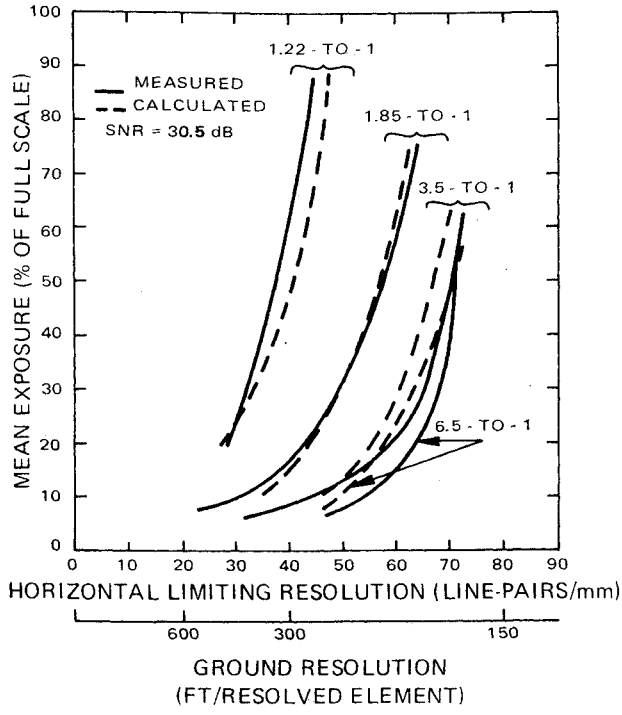

Fig. 10 Limiting resolution.

area under the curves, which is a measure of the information gathering capability of the cameras, remained essentially the same both with and without aperture correction of the video signal.

The ERTS-A spacecraft was placed in orbit on July 23, 1972, and operation of the RBV cameras began shortly after launch. Pictures were successfully received at both the U.S. and Canadian ground stations. Operation of the RBV cameras was terminated during early August 1972 as a result of a spacecraft

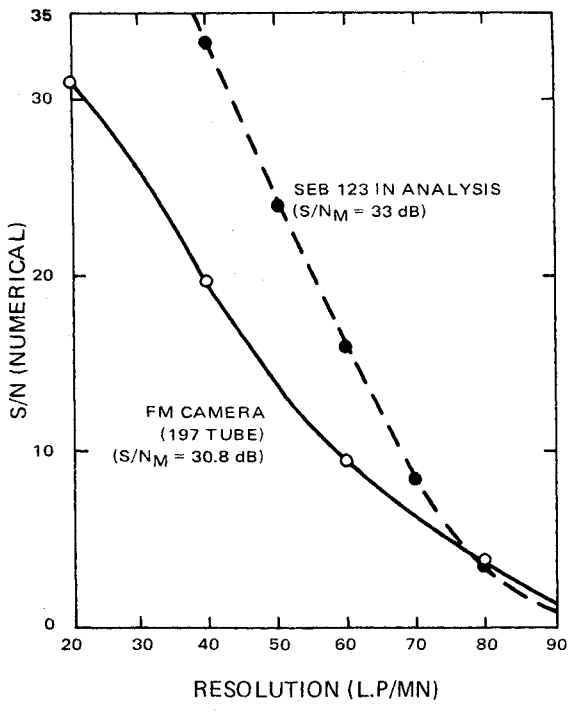

Fig. 11 Signal-to-noise ratio vs spatial frequency (channel 2, square wave inputs).

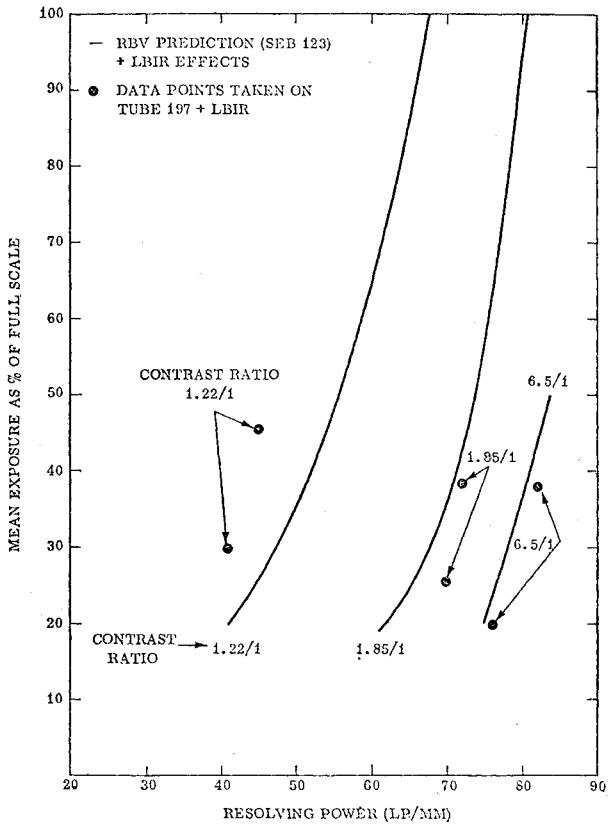

Fig. 12 Resolution vs exposure at various contrast ratios.

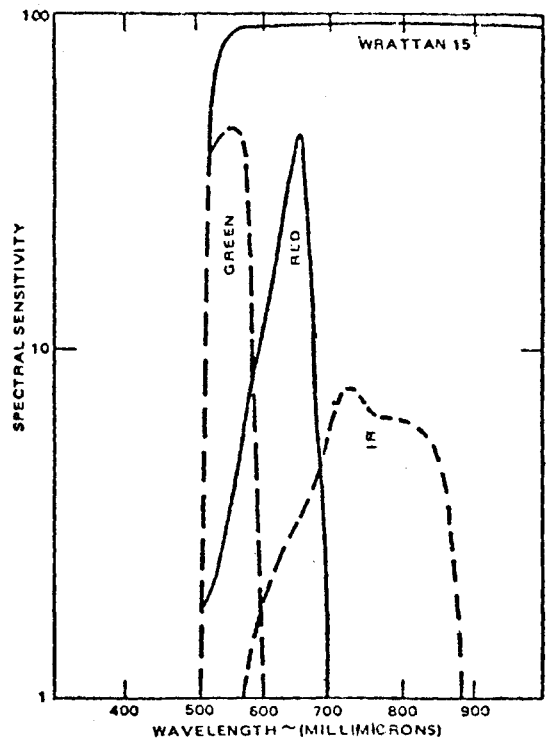

Fig. 13 Spectral characteristics of IR film (S0180).

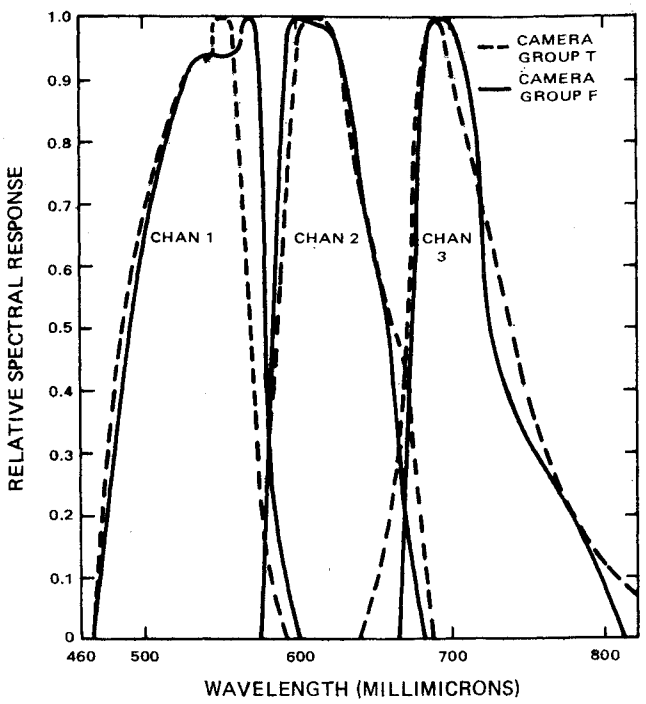

Fig. 14 Spectral response of cameras for Flights A and B.

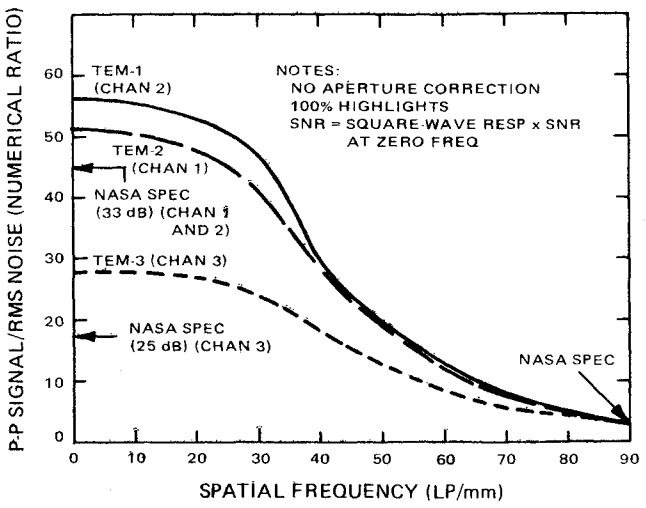

Fig. 15 SNR vs spatial frequency plot for Group T cameras.

anomaly. In this brief period hundreds of high quality pictures of the U.S., Canada, and other regions were obtained by the NASA Data Processing Center located at the Goddard Space Flight Center, Greenbelt, Md. A complete cataloging of the imagery received and processed by NASA during this period is contained in Refs. 12–17.

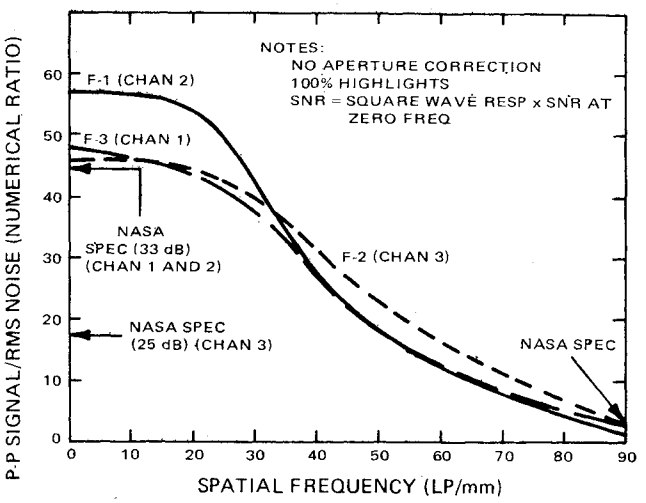

Fig. 16 SNR vs spatial frequency plot for Group F cameras.

References

[1] Miller, B. P., "Return-Beam Vidicon Multispectral Camera System for ERTS A and B," *Journal of the British Interplanetary Society*, Vol. 25, 1972, pp. 1–11.

[2] Norwood, V., "Optimization of a Multispectral Scanner for ERTS," *Proceedings of the Sixth International Symposium of Environment*, Vol. 1, Oct, 1969, Willow Run Lab., Univ. of Michigan, Ann Arbor, Mich.

[3] Earing, D. and Smith J., *Target Signature Analysis Center: Data Compilation*, Willow Run Lab., Univ. of Michigan, Ann Arbor, Mich., July 1966.

[4] Coltman, J. P. and Anderson, E. A., "Noise limitations to Resolving power in Electronic Imaging," *Proceedings of the IRE*, Vol. 48, May 1960, p. 858.

[5] Brock, G. et al., *Photographic Considerations for Aerospace*, Itek Corp., 1965, Lexington, Mass.

[6] Biberman, L. and Nudelman, S., eds., *Photoelectronic Imaging Devices*, Vol. 1, Plenum, New York, 1971, Chap. 11, pp. 245ff.

[7] Schade, O. H., "An Evaluation of photographic Image Quality and Resolving Power," *Journal of Society of Motion Picture and Television Engineers*, Vol. 73, Feb. 1964, pp. 81–119.

[8] Schade, O. H., "The Resolving-Power Functions and Quantum Processes of Television Cameras," *RCA Review*, Vol. 27, Sept. 1967, p. 460.

[9] Schade, O. H., "Image Gradation, Graininess and Sharpness in Television and Motion-Picture Systems, Part IV," *Journal of Society of Motion Picture and Television Engineers*, Vol. 64, Nov. 1955, pp. 593–617.

[10] Ravner, S., "Laser Beam Image Reproducer," *Proceedings of the SPSE Symposium on Electronic Imaging Systems*, April 15, 1970.

[11] Weinstein, O., Miller, B. P. and Barletta, J., "Simulation of ERTS RBV Imagery," *Proceedings of the Seventh International Symposium on Remote Sensing of the Environment*, Willow Run Lab. Univ, of Michigan, May 1971.

[12] Earth Resources Technology Satellite, *US Standard Catalog*, NASA Goddard Space Flight Center, Sept. 5, 1972.

[13] Earth Resources Technology Satellite, *US Standard Catalog*, NASA Goddard Space Flight Center, Sept. 23, 1972.

[14] Earth Resources Technology Satellite, *US Standard Catalog*, NASA Goddard Space Flight Center, Oct. 31, 1972.

[15] Earth Resources Technology Satellite, *Non-US Standard Catalog*, NASA Goddard Space Flight Center, Sept, 5, 1972.

[16] Earth Resources Technology Satellite, *Non-US Standard Catalog*, NASA Goddard Space Flight Center, Sept. 23, 1972.

[17] Earth Resources Technology Satellite, *Non-US Standard Catalog*, NASA Goddard Space Flight Center, Oct. 31 1972